Open Access

Joachim Greiner*, Stefan Pollnow, Steffen Schuler, Gustavo Lenis, Gunnar Seemann and Olaf Dössel

Simulation of intracardiac electrograms around acute ablation lesions

Abstract: Radiofrequency ablation (RFA) is a widely used clinical treatment for many types of cardiac arrhythmias. However, nontransmural lesions and gaps between linear lesions often lead to recurrence of the arrhythmia. Intracardiac electrograms (IEGMs) provide real-time information regarding the state of the cardiac tissue surrounding the catheter tip. Nevertheless, the formation and interpretation of IEGMs during the RFA procedure is complex and yet not fully understood. In this in-silico study, we propose a computational model for acute ablation lesions. Our model consists of a necrotic scar core and a border zone, describing irreversible and reversible temperature induced electrophysiological phenomena. These phenomena are modeled by varying the intra- and extracellular conductivity of the tissue as well as a regulating zone factor. The computational model is evaluated regarding its feasibility and validity. Therefore, this model was compared to an existing one and to clinical measurements of five patients undergoing RFA. The results show that the model can indeed be used to recreate IEGMs. We computed IEGMs arising from complex ablation scars, such as scars with gaps or two overlapping ellipsoid scars. For orthogonal catheter orientation, the presence of a second necrotic core in the near-field of a punctiform acute ablation lesion had minor impact on the resulting signal morphology. The presented model can serve as a base for further research on the formation and interpretation of IEGMs.

Keywords: acute ablation lesions; in-silico modelling; intracardiac electrograms; radiofrequency ablation.

---

*Corresponding author: Joachim Greiner, Institute of Biomedical Engineering, Karlsruhe Institute of Technology (KIT), Kaiserstr. 12, 76128 Karlsruhe, Germany, E-mail: publications@ibt.kit.edu
Stefan Pollnow, Steffen Schuler, Gustavo Lenis and Olaf Dössel: Institute of Biomedical Engineering, Karlsruhe Institute of Technology (KIT), Kaiserstr. 12, 76128 Karlsruhe, Germany
Gunnar Seemann: Institute for Experimental Cardiovascular Medicine, University Heart Center Freiburg – Bad Krozingen, Medical Center – University of Freiburg, Germany; and Medical Department, Albert-Ludwigs University, Freiburg, Germany, E-mail: gunnar.seemann@universitaets-herzzentrum.de

1 Introduction

Radiofrequency ablation (RFA) is the gold standard procedure for many forms of cardiac arrhythmias, including atrial fibrillation, when drug therapy is not effective. A corner stone for RFA success is the creation of transmural and continuous scars arising from elevated temperatures due to radiofrequency currents. Unfortunately, the recurrence rate of arrhythmias is relatively high at 35–45% [1], which means that patients often have to undergo a second procedure. However, to date, there are no reliable criteria for evaluating acute ablation lesions and monitoring the ablation process. Animal and clinical studies have shown that electrogram (EGM)-based criteria can be used to evaluate the formation of single point lesions [2, 3]. In this in-silico study, we investigated the influence of ablation lesions and catheter orientation on the morphology of intracardiac electrograms (IEGMs). We extended an existing model of an acute ablation lesion to cover more complex geometries; that is, those consisting of two point-shaped lesions. By evaluating the simulated IEGMs, new parameters can be identified to assess complex ablation lesions.

2 Methods

2.1 Simulation setup

For our in-silico studies, we solved the finite element bidomain formulation using the cardiac simulation framework acCELLerate [4]. We adapted our computational model of an acute ablation lesion from the model of Keller et al. [5]. The simulations were performed on an isotropic patch of myocardium with a size of $40\,mm \times 24\,mm \times 22\,mm$ and a spatial resolution of $0.2\,mm$. An 8F (2.7 mm) non-irrigated ablation catheter with an 8 mm distal electrode and a 1.2 mm proximal electrode was placed either orthogonally or parallel to the myocardium. The catheter tip deforms the tissue surface by 1 mm for the orthogonal orientation, whereas the parallel orientation results in no tissue deformation. An intracellular stimulus

Table 1: Overview of intra- and extracellular conductivities and CV for several temperature ranges.

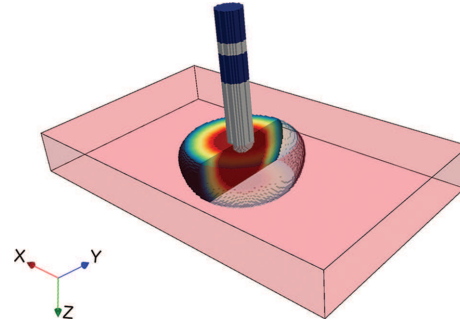| Material	σ_i (S/m)	σ_e (S/m)	CV (mm/s)
Myocardium	0.40	0.264	800
Blood	10^{-10}	0.70	–
Lesion (40–43°C)	0.47–0.53	0.264	844–873
Lesion (43–46°C)	0.53–0.36	0.264	873–784
Lesion (46–50°C)	0.36–0.01	0.264	784–160
Lesion (necrotic)	10^{-10}	0.10	–
Electrode	10^{-10}	$7 \cdot 10^3$	–
Isolation	10^{-10}	10^{-10}	–

The intracellular conductivity in the border zones is continuous and is given as the range of values in this zone. We assumed a membrane capacity C_m of 0.1 µF/cm^2 and surface to volume ratio β of 100 mm^{-1}.

Figure 1: Exemplary simulation setup for orthogonal catheter orientation. The whole setup is surrounded by blood (not shown in this figure). **Legend:** Acute border zone (50°C ▬▬▬▬ 40°C), necrotic scar core (▬), myocardium (▬), electrode (▬), isolation (▬).

current was applied at the left tissue boundary to initiate excitation propagation. The extracellular and intracellular conductivities of the myocardium were set to 0.264 S/m [6] and 0.40 S/m, respectively, which yielded a conduction velocity (CV) of 800 mm/s (see Table 1). According to Clayton et al. [7], both of these values are within the range of experimental measurements. The myocardium is completely surrounded by blood with an extracellular conductivity of 0.7 S/m and no intracellular conductivity [8]. The conductivity of the electrode was defined to be 10,000 times higher than the conductivity of blood, which resulted in a near-equipotential volume inside the metal. An isolating material was placed between the distal and proximal electrode. The boundaries of the intra- and extracellular domains were implemented with no-flux Neumann conditions and the following constraint was used to fix the extracellular potential ϕ_e:

$$\int_\Omega \phi_e \ d\Omega = 0. \tag{1}$$

2.2 Ablation models

Keller et al. [5] modeled an acute ablation lesion with a necrotic core and a border zone consisting of six different layers with properties of heated myocardium. We expanded this model to a continuous temperature distribution, where we calculated electrophysiological parameters uniquely for each voxel in the border zone. The action potential (AP) changes were modeled in a ten Tusscher cell model, which was adapted for ischemia phase 1a by Wilhelms et al. [5, 9]. The lesion model assumes a maximum scar width of 10 mm for orthogonal orientation (for parallel orientation: 12.8 mm) and a scar width to

depth ratio of 1.25 for orthogonal catheter orientation (for parallel orientation: 1.6) [5]. The intracellular conductivity of the necrotic scar core was set to zero and the extracellular conductivity was set to 0.1 S/m. We estimated the intracellular conductivity for each temperature using the findings of the hyperthermia experiments from Simmers et al. [10]. Subsequently, small patches of myocardium ($120 \times 30 \times 65$ voxel elements with a spatial resolution of 0.2 mm) were used to determine intracellular conductivities for different temperatures, while the corresponding extracellular conductivity remained constant. We calculated the CV by using the steepest point in the AP upstroke as reference point for cellular activation. CV over intracellular conductivity σ_i was then interpolated with cubic splines to obtain a function for CV (see Table 1). The second part of this study deals with a simplified in-silico model for complex ablation lesions. As a first approach, we assumed that the border zones of the first ablation lesion were completely cooled down by blood flow and heat loss due to local tissue perfusion. Inflammation as well as edemas were excluded in this model. The second ablation lesion was set along the x-axis of the first ablation scar. The distance between the center of both lesions was varied between 6.6 and 12.6 mm with a step-width of 2 mm, representing all important scar configurations from mostly overlapping scar cores to ablation lesions with gaps. If the passive necrotic core overlapped the border zones of the second lesion, necrotic tissue was assigned to this region.

2.3 Simulation and analysis of IEGMs

We referenced the simulated extracellular potentials with the tissue-distant top voxel layer of our computational setup. The bipolar EGM was obtained by subtracting the

Table 2: Relative changes during ablation in measured and simulated IEGMs characteristics (mean value and standard deviation).

Clinical IEGMs				Simulated IEGMs		
Orientation	Rel. maximum	Rel. minimum	Rel. derivative	Rel. maximum	Rel. minimum	Rel. derivative
Orthogonal, distal	-0.17 ± 0.27	-0.94 ± 0.10	-0.80 ± 0.09	-0.13 ± 0.00	-0.81 ± 0.00	-0.78 ± 0.00
Orthogonal, proximal	$-$	$-$	$-$	-0.04 ± 0.00	-0.64 ± 0.00	-0.49 ± 0.00
Orthogonal, bipolar	-0.95 ± 0.17	-0.20 ± 0.33	-0.79 ± 0.10	-0.87 ± 0.00	-0.33 ± 0.00	-0.81 ± 0.00
Parallel – DP, distal	-0.27 ± 0.53	-1.04 ± 0.14	-0.81 ± 0.05	-0.18 ± 0.00	-0.73 ± 0.00	-0.31 ± 0.00
Parallel – DP, proximal	-0.15 ± 0.23	-0.09 ± 0.53	0.09 ± 0.41	-0.52 ± 0.00	-0.23 ± 0.00	0.06 ± 0.00
Parallel – DP, bipolar	-1.06 ± 0.37	-0.14 ± 0.54	-0.24 ± 0.82	-0.73 ± 0.00	-0.27 ± 0.00	-0.04 ± 0.00
Parallel – PD, distal	-0.31 ± 0.21	-1.00 ± 0.12	-0.88 ± 0.10	-0.31 ± 0.00	-0.73 ± 0.00	-0.53 ± 0.00
Parallel – PD, proximal	-0.22 ± 0.21	-0.46 ± 0.12	-0.45 ± 0.19	0.09 ± 0.00	-0.20 ± 0.00	0.17 ± 0.00
Parallel – PD, bipolar	-0.59 ± 0.17	-0.39 ± 0.03	-0.46 ± 0.13	-0.80 ± 0.00	-0.25 ± 0.00	-0.25 ± 0.00

For parallel catheter orientation, we distinguished between distal to proximal (DP) and proximal to distal (PD) wave propagation.

proximal EGM from the distal EGM. In order to compare clinical measurements with simulated IEGMs, a transfer function with a first order butterworth highpass at 30 Hz and a first order butterworth lowpass at 250 Hz was used [5]. For comparison, we automatically annotated the following markers in the simulated data as well as from five patients undergoing RFA procedure in the right atrium: positive peak amplitude, negative peak amplitude and the maximum absolute first derivative between positive and negative peak. The deviation of computed IEGMs and clinical IEGMs was quantified by the deviation factor Q_V:

$$Q_V = \sum_{\forall i} \frac{1}{(\sigma_{clinical,i})^2} \cdot \left(E_{clinical,i} - E_{comp,i} \right)^2, \quad (2)$$

where $\sigma_{clinical}$ is the standard deviation and E is the mean value of each charactistic.

3 Results

Extracted quantified signal statistics are shown in Table 2. For orthogonal catheter orientation, extracted mean values are in high accordance with the distribution extracted from clinical IEGMs, resulting in relatively a small Q_V value of 2. For parallel catheter orientation with distal to proximal wave propagation, all mean values are in line with the clinical IEGMs, except the upstroke reduction in the distal IEGM. Therefore, Q_V results in a rather high value of 107. Proximal to distal wave propagation lead to a similar pattern, but with less total deviation, resulting in a Q_V value of 59.

In Figure 2, some of the simulated IEGMs are presented in their filtered state together with the clinical signals for orthogonal catheter orientation. For all cases only a slight change was determined in the proximal IEGM. Therefore, the changes in bipolar IEGMs were dominated by the distal
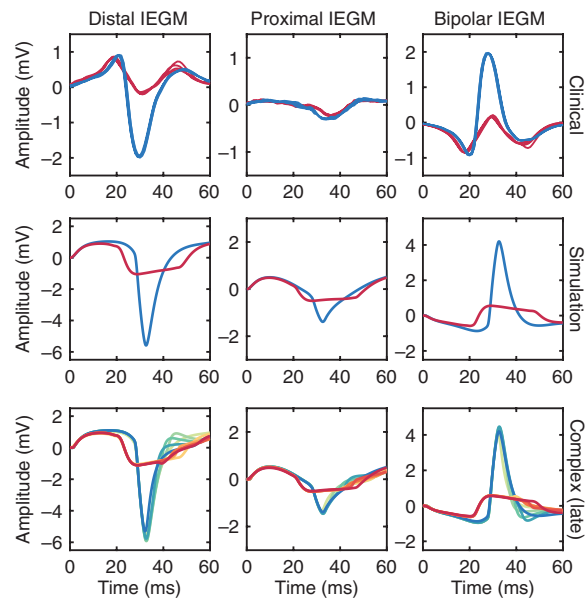
Figure 2: Comparison of filtered simulated IEGMs for point-shaped and complex ablation lesions, as well as clinical filtered IEGMs, before and after RFA, for orthogonal catheter orientation. **Scar Legend:** Point-shaped scars ( ), distance of complex scars (12.6 mm 6.6 mm, 12.6 mm 6.6 mm). **Time Legend:** Before ablation ( ), after ablation ( ).

IEGM. This relation was also present for parallel catheter orientation. For complex scars, the visualization goal is not to observe individual changes, but rather to grasp the overall minor changes in signal morphology. Neither the morphology of the IEGM, nor the extracted signal statistic showed major changes.

4 Discussion

In this computational study, we investigated the morphological changes of IEGMs shortly after the RFA

procedure. For this purpose, an existing model of an acute ablation lesion was developed further and subsequently, a first model of a complex ablation lesion was introduced. The in-silico experiments were performed with an 8F non-irrigated ablation catheter, which is often used in clinical ablation procedures. Additionally, the orientation of the ablation catheter and the distances between two ablation lesions were varied on the three-dimensional myocardial patch. This computational setup offered the possibility to evaluate the distal, proximal and bipolar IEGMs for varying lesion geometry and transmurality.

We compared the expanded model with the computational model from Keller et al. [5] and clinical signals during RFA procedures. Compared to the original model from [5], the deviation factor Q_V decreased from 513 to 167. Hereby, a better statistical agreement between our simulated IEGMs and the clinical IEGMs was found with the new ablation lesion model. The simulation setup of the complex ablation lesions was a first step to reproduce more realistic clinical ablation patterns consisting of several point-shaped lesions. With our simplified necrotic core-model it is not feasible to detect gaps between two ablation scars nor to identify correspondent markers in the IEGMs, especially in retrospect with the natural deviation range seen in the clinical data set. To the best of our knowledge, no computational model exist to investigate more complex acute ablation lesions and cardiac electrophysiology around these areas simultaneously. In a next step, we will implement further modular expansions to the ablation process. We can computationally substantiate many presumptions, such as heat distribution and bio-heat transfer, blood flow and applied contact-force. Moreover, non-irrigated or irrigated ablation catheters of different geometries could be investigated. Simulated IEGMs of this new model have to be compared with clinical signals of more complex ablation lesions, such as linear lesions. Hereby, we will evaluate the changes of the IEGMs to identify robust criteria for describing lesion geometry as well as transmurality.

Finally, we want to highlight that clinical filter parameters are usually overlooked when talking about IEGMs. Signal morphology is strongly dependent on the order as well as on the chosen cut-off frequencies of the filter and therefore, these parameters have to be carefully considered when comparing IEGMs.

References

[1] Shurrab M, Biase LD, Briceno DF, Kaoutskaia A, Haj-Yahia S, Newman D, et al. Impact of contact force technology on atrial fibrillation ablation: a meta-analysis. J Am Heart Assoc. 2015;4:e002476.

[2] Otomo K, Uno K, Fujiwara H, Isobe M, Iesaka Y. Local unipolar and bipolar electrogram criteria for evaluating the transmurality of atrial ablation lesions at different catheter orientations relative to the endocardial surface. Heart Rhythm. 2010;7:1291–300.

[3] Bortone A, Appetiti A, Bouzeman A, Maupas E, Ciobotaru V, Boulenc JM, et al. Unipolar signal modification as a guide for lesion creation during radiofrequency application in the left atrium: a prospective study in humans in the setting of paroxysmal atrial fibrillation catheter ablation. Circ Arrhythmia Electrophysiol. 2013;6:1095–102.

[4] Seemann G, Sachse FB, Karl M, Weiss DL, Heuveline V, Dössel O. Framework for modular, flexible and efficient solving the cardiac bidomain equation using PETSc. Progr Ind Math. 2010;15:363–9.

[5] Keller MW, Schuler S, Wilhelms M, Lenis G, Seemann G, Schmitt C, et al. Characterization of radiofrequency ablation lesion development based on simulated and measured intracardiac electrograms. IEEE Trans Biomed Eng. 2014;61:2467–78.

[6] Schwab BC, Seemann G, Lasher RA, Torres NS, Wulfers EM, Arp M, et al. Quantitative analysis of cardiac tissue including fibroblasts using three-dimensional confocal microscopy and image reconstruction: towards a basis for electro-physiological modeling. IEEE Trans Med Imaging. 2013;32: 862–72.

[7] Clayton RH, Bernus O, Cherry EM, Dierckx H, Fenton FH, Mirabella L, et al. Models of cardiac tissue electrophysiology: progress, challenges and open questions. Prog Biophys Mol Biol. 2011;104:22–48.

[8] Gabriel S, Lau RW, Gabriel C. The dielectric properties of biological tissues: III. parametric models for the dielectric spectrum of tissues. Phys Med Bio. 1996;41:2271.

[9] Wilhelms M, Dössel O, Seemann G. In silico investigation of electrically silent acute cardiac ischemia in the human ventricles. IEEE Trans Biomed Eng. 2011;58: 2961–4.

[10] Simmers TA, De Bakker JM, Wittkampf FH, Hauer RN. Effects of heating on impulse propagation in super-fused canine myocardium. J Amer Coll Cardiol. 1995;25: 1457–64.